



UNIVERSIDAD DISTRITAL
FRANCISCO JOSÉ DE CALDAS




Research

Dynamic Model of Lower Limb Motion in the Sagittal Plane during the Gait Cycle

Modelo dinámico del movimiento del miembro inferior en el plano sagital durante el ciclo de marcha

José Luis Sarmiento-Ramos¹  *, Andrés Felipe Meneses-Castro², and Pedro José Jaimes-Mantilla²

¹Rambal S.A.S BIC (Bucaramanga, Colombia). Universidad Santo Tomás 

²Universidad Manuela Beltrán (Bucaramanga, Colombia) 

Abstract

Context: This work presents the development of a dynamic model for human lower limb motion in the sagittal plane during the gait cycle. The primary objective of this model is to serve as a powerful tool for the design of rehabilitation and assistive devices, such as exoskeletons, prostheses, and orthoses. It achieves this by facilitating the estimation of joint torques, the detailed analysis of kinematic variables, optimal actuator selection, and the exploration of advanced control techniques.

Method: The dynamic model consists of two primary components: (1) the plant model and (2) a closed-loop controller. The plant model represents the forward dynamics of human gait and is based on a multi-mass pendulum composed of three segments of the lower limb (thigh, lower leg, and foot) and three joints (hip, knee, and ankle). It is analyzed using the Euler-Lagrange formulation and the nonlinear second-order differential equations are implemented in MATLAB's Simulink. To reproduce reference human gait trajectories and simulate the functioning of the neuromusculoskeletal system and the central nervous system, a closed-loop PID controller is incorporated into the plant model. It is noteworthy that the scope of this dynamic model is specifically confined to the sagittal plane.

Results: The dynamic model is evaluated in terms of angular displacement tracking using the relative maximum error (RME) and the root mean square error (RMSE) for reference trajectories of healthy adult male human gait as reported in the literature. The model demonstrates tracking with errors below 2.2 [°] in magnitude and 3,5% for all three considered segments (thigh, lower leg, and foot).

Conclusions: The quantitative results show that the dynamic model developed in this work is reliable and allows for a precise reproduction of human gait trajectories.

Keywords: biomechanics, Euler-Lagrange, human gait, PID control, Simulink

Article history

Received:
11th/Jan/2023

Modified:
19th/sep/2023


Accepted:
10th/Oct/2023

Ing, vol. 29, no. 1,
2024. e20333

©The authors;
reproduction right
holder Universidad
Distrital Francisco
José de Caldas.

Open access



*  Correspondence: joseluis_251094@hotmail.com

Resumen

Contexto: Este trabajo presenta el desarrollo de un modelo dinámico del movimiento del miembro inferior humano en el plano sagital durante el ciclo de marcha. El objetivo principal de este modelo es servir como una herramienta poderosa para el diseño de dispositivos de rehabilitación y asistencia, como exoesqueletos, prótesis y órtesis. Esto lo logra facilitando la estimación de torques en las articulaciones, el análisis detallado de variables cinemáticas, la selección óptima de actuadores y la exploración de técnicas avanzadas de control.

Método: El modelo dinámico se consiste en dos componentes principales: (1) el modelo de la planta y (2) un controlador de lazo cerrado. El modelo de la planta representa la dinámica directa de la marcha humana y se basa en un péndulo de múltiples masas compuesto por tres segmentos del miembro inferior (muslo, pantorrilla y pie) y tres articulaciones (cadera, rodilla y tobillo). Este es analizado utilizando la formulación de Euler-Lagrange y las ecuaciones diferenciales de segundo orden no lineales se implementan en Simulink de MATLAB. Para reproducir las trayectorias de referencia de la marcha humana y simular el funcionamiento del sistema musculoesquelético y del sistema nervioso central, se implementa un controlador PID de lazo cerrado en el modelo de la planta. Es importante destacar que el alcance de este modelo dinámico se limita específicamente al plano sagital.

Resultados: El modelo dinámico es evaluado en términos del seguimiento del desplazamiento angular usando el error relativo máximo (RME) y el error medio cuadrático (RMSE) para trayectorias de referencia de la marcha humana de adultos masculinos sanos reportadas en la literatura. El modelo demuestra un seguimiento con errores por debajo de 2.2 [°] en magnitud y 3,5% para los tres segmentos considerados (muslo, pantorrilla y pie).

Conclusiones: Los resultados cuantitativos muestran que el modelo dinámico desarrollado en este trabajo es confiable y permite reproducir precisamente las trayectorias de la marcha humana.

Palabras clave: biomecánica, Euler-Lagrange, marcha humana, control PID, Simulink

Table of contents

		2.2. Closed-loop controller	9
	Page	3. Simulations and results	12
1. Introduction	2	4. Conclusions	14
2. Dynamic model	5	5. Author contributions	16
2.1. Plant model	5	References	16

1. Introduction

Gait, also referred to as bipedal locomotion, is a cyclic and fundamental movement that involves a sequence of repetitive events, initiating and concluding with the contact of the initial foot with the ground. This dynamic process encompasses a steady-state gait cycle, comprising the stance phase (when the reference foot is on the ground) and the swing phase (when the reference foot is off the

ground). Gait constitutes a complex functional task that necessitates intricate coordination between numerous major joints within the human body, with particular emphasis on the lower limb (1).

The modeling of human gait has garnered substantial attention from researchers in recent decades due to its profound implications in biomedical engineering. This interest arises from its applications in designing rehabilitation and assistive devices, as well as analyzing abnormal gait patterns and their consequences. Currently, the design of such devices, including exoskeletons, prostheses, and orthoses, often relies on empirical and trial-and-error approaches. Many of these devices are constructed and subsequently tested on individuals before obtaining valuable feedback, resulting in an inefficient and costly design process. Dynamic models provide a robust tool for designers by enabling the estimation of crucial kinematic and kinetic variables, such as angular displacements, velocities, accelerations, joint torques, and muscle forces. This facilitates optimal actuator selection and in-depth investigation into control techniques in order to achieve satisfactory performance before implementation (2–4). A rigorous and precise modeling approach enables the extrapolation of simulation results into practical applications, allowing designers to thoroughly evaluate their devices in a virtual environment before prototyping and human testing, thus reducing risks and costs (5). Additionally, dynamic modeling serves as a valuable resource for clinicians, rehabilitation experts, and researchers, enhancing their comprehension of both normal and pathological gait patterns and assisting in the identification of causes and effects related to abnormal movement patterns. A comprehensive understanding of the gait cycle, its parameters, and the principles underlying the musculoskeletal system and the central nervous system (CNS) provides essential insights for evaluating and treating locomotion dysfunctions in clinical environments (1).

Research regarding the dynamic modelling of human gait can be categorized into two main fields: (1) musculoskeletal models and (2) biped robotics models. Musculoskeletal models (6) focus on the interaction and contributions of individual muscles, tendons, and ligaments during gait, emphasizing in the physiological aspects of bipedal locomotion. These models are highly intricate and computationally intensive, given their numerous degrees of freedom (DOF), diverting attention from the fundamental dynamics of the human gait. In contrast, biped robotics models aim at real-time gait control and the evaluation of kinematic and kinetic variables of joints and body segments. According to (7), biped robotics models can be divided into five groups: (1) pendulum models, (2) passive dynamic walkers, (3) zero-moment-point (ZMP) methods, (4) optimization-based methods, and (5) control-based methods.

Pendulum models are based on the principle of energy conservation, capturing the exchange between the kinetic and potential energy inherent in walking. Research in this area ranges from simple planar (8,9) to 3D (10,11) and multi-mass pendulum models (12,13). Pendulum models offer advantages in terms of simplicity, closed-form analytical solutions, and their ability to represent energy exchange principles during gait. However, they can oversimplify dynamics when certain joints and segments, such as the knee, ankle, lower leg, or foot, are not explicitly considered.

Passive dynamic walkers (14–16) are biped models that emulate a compass-like mechanism driven purely by gravity as they descend gentle slopes. These models do not involve any actuation or control of

joint angles or torques at any point. During their descent, the leg follows a pendulum-like trajectory, and the swing foot's contact with the ground is dictated by the conservation of angular momentum. Passive dynamic walkers are simple and efficient models suitable for investigating the fundamental principles of human gait, including the relationship between step length and velocity, energy expenditure, and the transition from walking to running. However, like pendulum-based models, they may oversimplify dynamics by neglecting certain joints and segments.

ZMP methods (17–19) focus on achieving bipedal walking by enforcing the body's balance to follow predefined locations. Each ZMP represents a point on the ground where the net moment of active forces, including inertia, gravity, and external forces from actuators, is zero. The dynamic equations in this approach primarily serve to ensure balance constraints rather than coordinate the entire gait trajectory. ZMP methods are computationally efficient for the real-time control of biped robots. However, it is essential to note that preplanned ZMP locations do not precisely mimic human walking principles or the CNS's control of gait.

Optimization-based methods (7, 20, 21) are computational approaches that seek to uncover the criteria governing human gait generation by the CNS. In these methods, the objective function – intended for optimization – typically represents a gait-related performance measure, such as dynamic effort, mechanical energy, metabolic energy, jerk, or stability. Constraints encompass the joint range of motion (ROM) and maximum joint torques. These methods offer insights into the relationship between gait and performance measures, shedding light on the working principles of human walking. However, they demand significant computational resources, are not well-suited for real-time applications, and rely on experimental data.

Control-based methods are deployed in humanoid robots to facilitate bipedal walking, allowing for interaction with the environment, responses to external disturbances, and real-time task execution. This approach closely approximates the natural control mechanisms of the human CNS, ensuring accurate analysis, estimation, and tracking of normal and pathological gait motions. Control-based methods can be classified into three categories: (1) tracking control, (2) optimal control, and (3) predictive control. Tracking control (22,23) involves calculating input forces or torques required to achieve desired walking trajectories for body segments using kinematic feedback. In optimal control approaches (24, 25), input forces or torques are treated as unknown variables in motion equations and are continuously optimized for the subsequent time step, also employing kinematic feedback. Predictive control methods (5, 22) are rooted in iterative finite horizon optimization, where online calculations are used to determine input forces or torques. This process minimizes a cost function incorporating kinematic feedback.

This paper introduces a dynamic model of human lower limb motion in the sagittal plane during the gait cycle. This model falls under the category of biped robotics and represents a hybrid approach incorporating elements of both pendulum and control-based methods. The model comprises two primary components: (1) the plant model, founded on a multi-mass pendulum, and (2) a closed-loop PID controller. The plant model captures the forward dynamics of human gait, employing the Euler-Lagrange formulation while considering the lower limb as consisting of three segments (thigh,

lower leg, and foot) and three joints (hip, knee, and ankle). The PID controller is integrated to estimate the joint torques necessary for replicating human gait reference trajectories. It constitutes a potent tool for the design of rehabilitation and assistive devices, facilitating joint torque estimation, kinematic variable analysis, optimal actuator selection, and the exploration of control techniques.

2. Dynamic model

As mentioned in the introduction, the dynamic model proposed for human lower limb motion encompasses two essential components: (1) the plant model and (2) a closed-loop PID controller. The plant model (the core of the dynamic model) represents the forward dynamics of human gait, and the closed loop controller simulates the working principle of the neuromusculoskeletal system and the CNS.

It is worth noting that the scope of this dynamic model is specifically confined to the sagittal plane. This deliberate limitation stems from the recognition that the motion and dynamic effects of the lower limb within the frontal and transverse planes exhibit diminished relevance compared to those within the sagittal plane (1).

2.1. Plant model

The plant model, responsible for capturing the dynamics of human lower limb motion, is meticulously formulated using the Euler-Lagrange formulation. This mathematical framework is applied to the system depicted in Fig. 1, which comprises three lower limb segments (thigh, lower leg, and foot) interconnected by three joints (hip, knee, and ankle). Each of the lower limb segments is modeled as a rigid bar by specific attributes. These attributes include length L_n , mass m_n , and the proximal gravity center l_n . These segments are positioned at angular positions θ_n relative to the vertical axis. To distinguish between the individual segments within the model, subscripts are employed as follows: '1' for the thigh, '2' for the lower leg, and '3' for the foot. The foundation of this modeling framework is established in a fixed coordinate system with its origin situated at the hip joint.

The Lagrangian L is established as the difference between the system's kinetic energy T and its potential energy V :

$$L = T - V \quad (1)$$

The kinetic energy is defined by Eq. (2), which incorporates the kinetic energy of each individual segment. In this equation, v_n represents the linear velocity, J_n denotes the moment of inertia, and $\dot{\theta}_n$ represents the angular velocity.

$$T = \frac{m_1 v_1^2}{2} + \frac{J_1 \dot{\theta}_1^2}{2} + \frac{m_2 v_2^2}{2} + \frac{J_2 \dot{\theta}_2^2}{2} + \frac{m_3 v_3^2}{2} + \frac{J_3 \dot{\theta}_3^2}{2} \quad (2)$$

The linear velocity can be expressed as the magnitude of the first derivative of the position vector r_n of the gravity center for each segment: $v_n = |\dot{r}_n|$. The centers of gravity for the thigh, lower leg, and foot are situated at positions r_1 , r_2 and r_3 , respectively:

$$r_1 = \begin{bmatrix} l_1 \sin \theta_1 \\ -l_1 \cos \theta_1 \end{bmatrix} \quad (3)$$

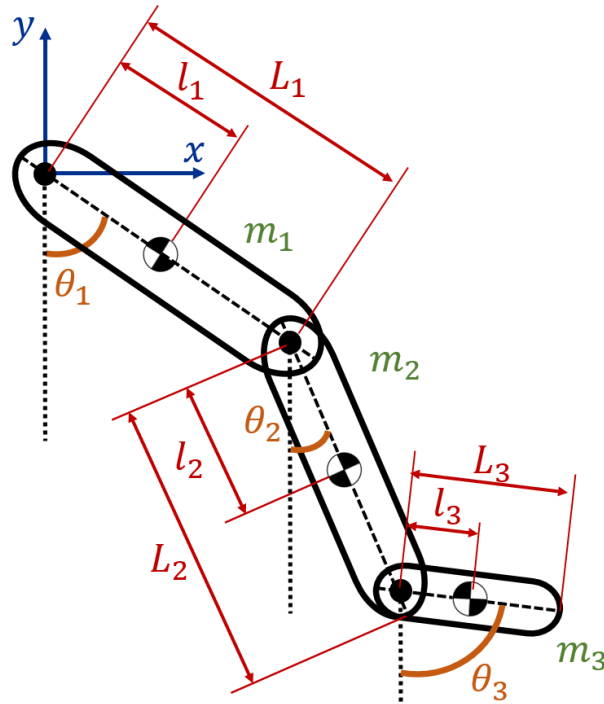


Figure 1. Representation of human lower limb for dynamic modeling

$$r_2 = \begin{bmatrix} L_1 \sin \theta_1 + l_2 \sin \theta_2 \\ -L_1 \cos \theta_1 - l_2 \cos \theta_2 \end{bmatrix} \quad (4)$$

$$r_3 = \begin{bmatrix} L_1 \sin \theta_1 + L_2 \sin \theta_2 + l_3 \sin \theta_3 \\ -L_1 \cos \theta_1 - L_2 \cos \theta_2 - l_3 \cos \theta_3 \end{bmatrix} \quad (5)$$

Therefore, the linear velocities of the thigh, lower leg, and foot are established as:

$$v_1 = \dot{\theta}_1 l_1 \quad (6)$$

$$v_2 = \sqrt{\dot{\theta}_1^2 L_1^2 + \dot{\theta}_2^2 l_2^2 + 2\dot{\theta}_1 \dot{\theta}_2 L_1 l_2 \cos(\theta_1 - \theta_2)} \quad (7)$$

$$v_3 = \sqrt{\dot{\theta}_1^2 L_1^2 + \dot{\theta}_2^2 L_2^2 + \dot{\theta}_3^2 l_3^2 + 2\dot{\theta}_1 \dot{\theta}_2 L_1 L_2 \cos(\theta_1 - \theta_2) + 2\dot{\theta}_2 \dot{\theta}_3 L_2 l_3 \cos(\theta_2 - \theta_3) + 2\dot{\theta}_1 \dot{\theta}_3 L_1 l_3 \cos(\theta_1 - \theta_3)} \quad (8)$$

Substituting Eqs. (6), (7), and (8) into (2) results in the following expression for the kinetic energy of the system:

$$\begin{aligned} T = & \frac{m_1 \dot{\theta}_1^2 l_1^2}{2} + \frac{J_1 \dot{\theta}_1^2}{2} + \frac{m_2 \dot{\theta}_1^2 L_1^2}{2} + \frac{m_2 \dot{\theta}_2^2 l_2^2}{2} + m_2 \dot{\theta}_1 \dot{\theta}_2 l_1 l_2 \cos(\theta_1 - \theta_2) + \frac{J_2 \dot{\theta}_2^2}{2} \\ & + \frac{m_3 \dot{\theta}_1^2 L_1^2}{2} + \frac{m_3 \dot{\theta}_2^2 L_2^2}{2} + \frac{m_3 \dot{\theta}_3^2 l_3^2}{2} + m_3 \dot{\theta}_1 \dot{\theta}_2 L_1 L_2 \cos(\theta_1 - \theta_2) \\ & + m_3 \dot{\theta}_2 \dot{\theta}_3 L_2 l_3 \cos(\theta_2 - \theta_3) + m_3 \dot{\theta}_1 \dot{\theta}_3 L_1 l_3 \cos(\theta_1 - \theta_3) + \frac{J_3 \dot{\theta}_3^2}{2} \end{aligned} \quad (9)$$

The potential energy is defined by Eq. (10), which incorporates the potential energy of each individual segment. In this equation, g denotes the gravity, and h_n represents the height of the center of gravity relative to the coordinate system.

$$V = m_1gh_1 + m_2gh_2 + m_3gh_3 \quad (10)$$

The height of the center of gravity for the thigh, lower leg, and foot can be expressed in terms of the angular displacement as:

$$h_1 = -l_1 \cos \theta_1 \quad (11)$$

$$h_2 = -L_1 \cos \theta_1 - l_2 \cos \theta_2 \quad (12)$$

$$h_3 = -L_1 \cos \theta_1 - L_2 \cos \theta_2 - l_3 \cos \theta_3 \quad (13)$$

Substituting Eqs. (11), (12), and (13) into (10) results in the following expression for the potential energy of the system:

$$V = -m_1gl_1 \cos \theta_1 - m_2gL_1 \cos \theta_1 - m_2gl_2 \cos \theta_2 - m_3gL_1 \cos \theta_1 - m_3gL_2 \cos \theta_2 - m_3gl_3 \cos \theta_3 \quad (14)$$

Eqs. (9) and (14) are substituted into (1) to obtain the Lagrangian of the system:

$$\begin{aligned} T = & \frac{m_1\dot{\theta}_1^2 l_1^2}{2} + \frac{J_1\dot{\theta}_1^2}{2} + \frac{m_2\dot{\theta}_1^2 L_1^2}{2} + \frac{m_2\dot{\theta}_2^2 l_2^2}{2} + m_2\dot{\theta}_1\dot{\theta}_2 l_1 l_2 \cos(\theta_1 - \theta_2) + \frac{J_2\dot{\theta}_2^2}{2} \\ & + \frac{m_3\dot{\theta}_1^2 L_1^2}{2} + \frac{m_3\dot{\theta}_2^2 L_2^2}{2} + \frac{m_3\dot{\theta}_3^2 l_3^2}{2} + m_3\dot{\theta}_1\dot{\theta}_2 L_1 L_2 \cos(\theta_1 - \theta_2) \\ & + m_3\dot{\theta}_2\dot{\theta}_3 L_2 l_3 \cos(\theta_2 - \theta_3) + m_3\dot{\theta}_1\dot{\theta}_3 L_1 l_3 \cos(\theta_1 - \theta_3) + \frac{J_3\dot{\theta}_3^2}{2} \\ & + m_1gl_1 \cos \theta_1 + m_2gL_1 \cos \theta_1 + m_2gl_2 \cos \theta_2 + m_3gL_1 \cos \theta_1 \\ & + m_3gL_2 \cos \theta_2 + m_3gl_3 \cos \theta_3 \end{aligned} \quad (15)$$

The Euler-Lagrange formulation is established by Eq. (16), where k represents the DOF, q_k the set of generalized coordinates, and Q_k the set of external (non-conservative) forces applied to the system. In the context of the system under consideration, there are three DOF associated with the three joints of the lower limb. The external forces encompass the torque T_n acting at each joint and the viscous damping, with b_n representing the viscous damping coefficient. The Euler-Lagrange formulation is applied as seen in Eqs. (17), (18), and (19) for the hip, knee, and ankle, respectively.

$$\frac{d}{dt} \left(\frac{\partial L}{\partial \dot{q}_k} \right) - \frac{\partial L}{\partial q_k} = Q_k \quad (16)$$

$$\frac{d}{dt} \left(\frac{\partial L}{\partial \dot{\theta}_1} \right) - \frac{\partial L}{\partial \theta_1} = T_1 - b_1\dot{\theta}_1 - b_2(\dot{\theta}_1 - \dot{\theta}_2) \quad (17)$$

$$\frac{d}{dt} \left(\frac{\partial L}{\partial \dot{\theta}_2} \right) - \frac{\partial L}{\partial \theta_2} = T_2 - b_2(\dot{\theta}_2 - \dot{\theta}_1) - b_3(\dot{\theta}_2 - \dot{\theta}_3) \quad (18)$$

$$\frac{d}{dt} \left(\frac{\partial L}{\partial \dot{\theta}_3} \right) - \frac{\partial L}{\partial \theta_3} = T_3 - b_3(\dot{\theta}_3 - \dot{\theta}_2) \quad (19)$$

The equations above are solved resulting in the nonlinear second-order differential Eqs. (20), (21), and (22), which describe the motion of the thigh, lower leg, and foot, respectively.

$$\begin{aligned}
& \ddot{\theta}_1(m_1l_1^2 + m_2L_1^2 + m_3L_1^2 + J_1) + \ddot{\theta}_2[m_2L_1l_2 \cos(\theta_1 - \theta_2) + m_3L_1l_2 \cos(\theta_1 - \theta_2)] \\
& + \ddot{\theta}_3[m_3L_1l_3 \cos(\theta_1 - \theta_3)] \\
& + \dot{\theta}_2^2[m_2L_1l_2 \sin(\theta_1 - \theta_2) + m_3L_1L_2 \sin(\theta_1 - \theta_2)] \\
& + \dot{\theta}_3^2[m_3L_1l_3 \sin(\theta_1 - \theta_3)] + m_1gl_1 \sin \theta_1 + m_2gL_1 \sin \theta_1 \\
& + m_3gL_1 \sin \theta_1 = T_1 - b_1\dot{\theta}_1 - b_2(\dot{\theta}_1 - \dot{\theta}_2)
\end{aligned} \tag{20}$$

$$\begin{aligned}
& \ddot{\theta}_2(m_2l_2^2 + m_3L_2^2 + J_2) + \ddot{\theta}_1[m_2L_1l_2 \cos(\theta_1 - \theta_2) + m_3L_1l_2 \cos(\theta_2 - \theta_3)] \\
& + \ddot{\theta}_3[m_3L_2l_3 \cos(\theta_2 - \theta_3)] \\
& + \dot{\theta}_1^2[-m_2L_1l_2 \sin(\theta_1 - \theta_2) - m_3L_1L_2 \sin(\theta_1 - \theta_2)] \\
& + \dot{\theta}_3^2[m_3L_2l_3 \sin(\theta_2 - \theta_3)] + m_2gl_2 \sin \theta_2 + m_3gL_2 \sin \theta_2 \\
& = T_2 - b_2(\dot{\theta}_2 - \dot{\theta}_1) - b_3(\dot{\theta}_2 - \dot{\theta}_3)
\end{aligned} \tag{21}$$

$$\begin{aligned}
& \ddot{\theta}_3(m_3l_3^2 + J_3) + \ddot{\theta}_2[m_3L_2l_3 \cos(\theta_2 - \theta_3)] + \ddot{\theta}_1[m_3L_1l_3 \cos(\theta_1 - \theta_3)] \\
& + \dot{\theta}_2^2[-m_3L_2l_3 \sin(\theta_2 - \theta_3)] + \dot{\theta}_1^2[-m_3L_1l_3 \sin(\theta_1 - \theta_3)] \\
& + m_2gl_3 \sin \theta_3 = T_3 - b_3(\dot{\theta}_3 - \dot{\theta}_2)
\end{aligned} \tag{22}$$

To simplify the aforementioned differential equations, certain parameters are combined into the following constants: $c_1 = m_1l_2 + m_2L_1^2 + m_3L_1^2 + J_1$, $c_2 = m_2L_1l_2$, $c_3 = m_3L_1L_2$, $c_4 = m_3L_1l_3$, $c_5 = m_1gl_1$, $c_6 = m_2gL_1$, $c_7 = m_3gL_1$, $c_8 = m_2l_2^2 + m_3L_2^2 + J_2$, $c_9 = m_3L_2l_3$, $c_{10} = m_2gl_2$, $c_{11} = m_3gL_2$, $c_{12} = m_3l_3^2 + J_3$, and $c_{13} = m_3gl_3$. As a result of these simplifications, Eqs. (23), (24), and (25) are obtained.

$$\begin{aligned}
& c_1\ddot{\theta}_1 + (c_2 + c_3)\ddot{\theta}_2 \cos(\theta_1 - \theta_2) + c_4\ddot{\theta}_3 \cos(\theta_1 - \theta_3) + (c_2 + c_3)\dot{\theta}_2^2 \sin(\theta_1 - \theta_2) \\
& + c_4\dot{\theta}_3^2 \sin(\theta_1 - \theta_3) + c_5 \sin \theta_1 + c_6 \sin \theta_1 + c_7 \sin \theta_1 \\
& = T_1 - b_1\dot{\theta}_1 - b_2(\dot{\theta}_1 - \dot{\theta}_2)
\end{aligned} \tag{23}$$

$$\begin{aligned}
& c_8\ddot{\theta}_2 + (c_2 + c_3)\dot{\theta}_1 \cos(\theta_1 - \theta_2) + c_9\ddot{\theta}_3 \cos(\theta_2 - \theta_3) - (c_2 + c_3)\dot{\theta}_1^2 \sin(\theta_1 - \theta_2) \\
& + c_9\dot{\theta}_3^2 \sin(\theta_2 - \theta_3) + c_{10} \sin \theta_2 + c_{11} \sin \theta_2 \\
& = T_2 - b_2(\dot{\theta}_2 - \dot{\theta}_1) - b_3(\dot{\theta}_2 - \dot{\theta}_3)
\end{aligned} \tag{24}$$

$$\begin{aligned}
& c_{12}\ddot{\theta}_3 + c_9\ddot{\theta}_2 \cos(\theta_2 - \theta_3) + c_4\ddot{\theta}_1 \cos(\theta_1 - \theta_3) - c_9\dot{\theta}_2^2 \sin(\theta_2 - \theta_3) - c_4\dot{\theta}_1^2 \sin(\theta_1 - \theta_3) \\
& + c_{13} \sin \theta_3 = T_3 - b_3(\dot{\theta}_3 - \dot{\theta}_1)
\end{aligned} \tag{25}$$

Eqs. (23), (24), and (25) are solved for the highest order derivatives $\ddot{\theta}_1$, $\ddot{\theta}_2$, and $\ddot{\theta}_3$ respectively, in order to obtain the following set of motion equations:

$$\begin{aligned} \ddot{\theta}_1 = \frac{1}{c_1} & \left[- \left((c_2 + c_3)\ddot{\theta}_2 \cos(\theta_1 - \theta_2) - c_4\ddot{\theta}_3 \cos(\theta_1 - \theta_3) \right) - (c_2 + c_3)\dot{\theta}_2^2 \sin(\theta_1 - \theta_2) \right. \\ & \left. - c_4\dot{\theta}_3^2 \sin(\theta_1 - \theta_3) - (c_5 + c_6 + c_7) \sin \theta_1 + T_1 - b_1\dot{\theta}_1 - b_2(\dot{\theta}_1 - \dot{\theta}_2) \right] \end{aligned} \quad (26)$$

$$\begin{aligned} \ddot{\theta}_2 = -\frac{1}{c_8} & \left[-(c_2 + c_3)\ddot{\theta}_1 \cos(\theta_1 - \theta_2) - c_9\ddot{\theta}_3 \cos(\theta_2 - \theta_3) + (c_2 + c_3)\dot{\theta}_1^2 \sin(\theta_1 - \theta_2) \right. \\ & \left. - c_9\dot{\theta}_3^2 \sin(\theta_2 - \theta_3) - (c_{10} + c_{11}) \sin \theta_2 + T_2 - b_2(\dot{\theta}_2 - \dot{\theta}_1) - b_3(\dot{\theta}_2 - \dot{\theta}_3) \right] \end{aligned} \quad (27)$$

$$\begin{aligned} \ddot{\theta}_3 = \frac{1}{c_{12}} & \left[-c_9\ddot{\theta}_2 \cos(\theta_2 - \theta_3) - c_4\ddot{\theta}_1 \cos(\theta_1 - \theta_3) + c_9\dot{\theta}_2^2 \sin(\theta_2 - \theta_3) \right. \\ & \left. + c_4\dot{\theta}_1^2 \sin(\theta_1 - \theta_3) - c_{13} \sin \theta_3 + T_3 - b_3(\dot{\theta}_3 - \dot{\theta}_1) \right] \end{aligned} \quad (28)$$

This plant model of human lower limb motion in the sagittal plane was implemented in MATLAB's Simulink, and it utilizes the non-linear second-order differential Eqs. (26), (27), and (28), as illustrated in the block diagram presented in Fig. 2. The inputs to this model consist of the joint torques (T_1 , T_2 and T_3) measured in units of $[N \cdot m]$, while the outputs are the angular displacements of the thigh, lower leg, and foot (θ_1 , θ_2 and θ_3), reported in units of $[rad]$.

The parameters that make up the plant model are detailed in Table I. These parameters are derived through an anthropometric analysis that relies on two primary factors: the body mass M and the height H of the individual. The mass of each segment and its corresponding length are linked to the individual's body mass and height, and the gravity center and radius of gyration are associated with the segment length (26,27).

2.2. Closed-loop controller

The neuromusculoskeletal system was conceptualized within a closed-loop feedback control scheme. In this structured framework, the body's segments and joints comprise the plant, muscles serve as the actuators, and an array of sensors, including proprioceptive and tactile sensors alongside visual and vestibular systems, act as sensory inputs. Overseeing this complex system is the CNS, functioning as the controller (28). The CNS receives input signals representing desired positions or reference trajectories, generated by the brain. These inputs are compared against real-time segment locations to compute tracking errors, which, in turn, guide the CNS in sending neural signals to muscles. These signals prompt the exertion of forces on the skeletal system, thereby producing joint torques to achieve the desired motion.

To simulate the neuromusculoskeletal system and the CNS, the model employs three angular displacement feedback PID controllers for the hip, knee, and ankle. Fig. 3 illustrates these controllers. Their inputs are tracking errors, computed as the difference between reference trajectories and actual

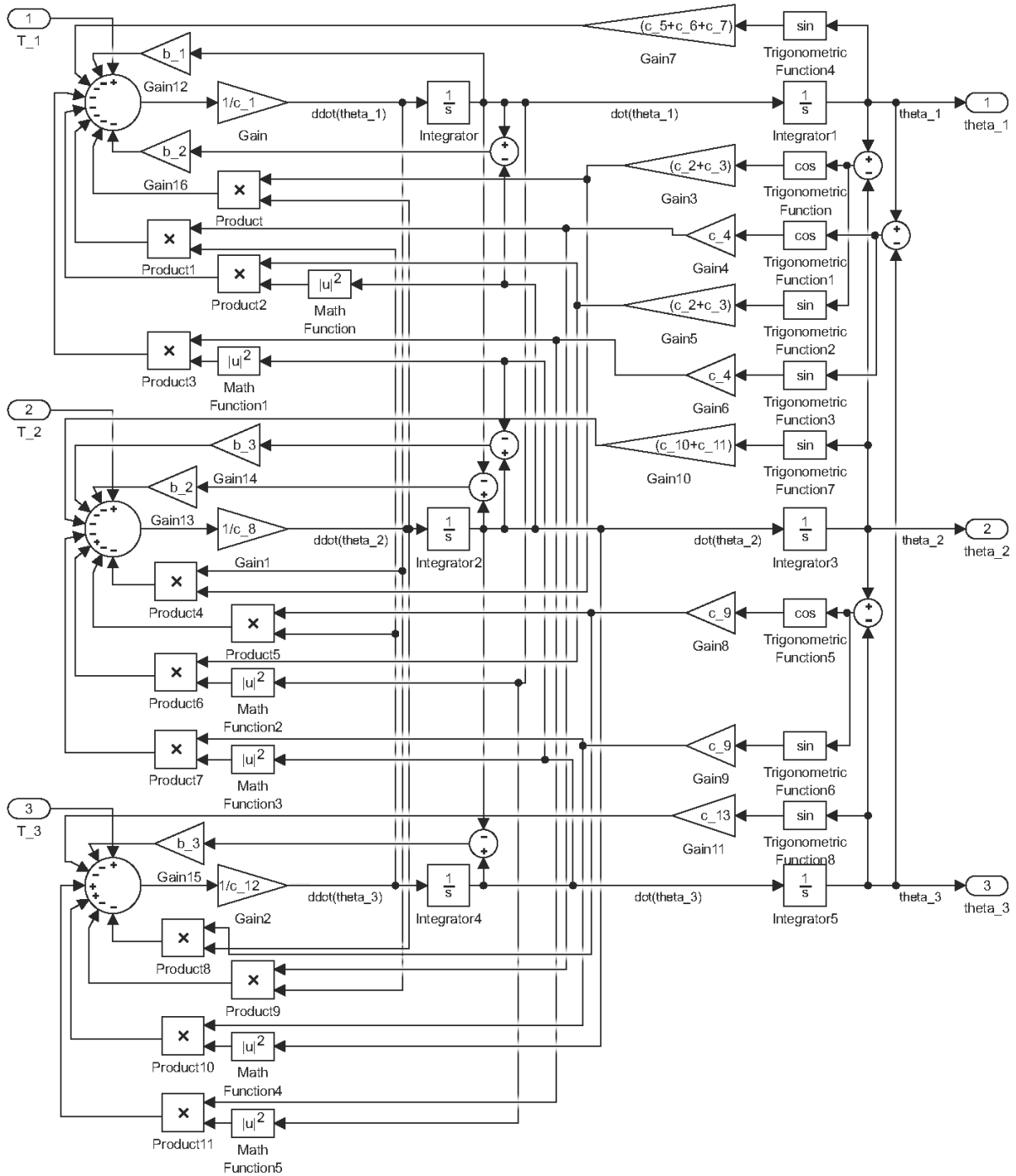


Figure 2. Plant model of human lower limb motion in Simulink

segment angular displacements. The controllers' outputs represent the joint torques required for carrying out the intended motion. These PID controller outputs feed directly into the plant model, depicted in Fig. 2. For the sake of clarity and comprehensibility, this plant model is encapsulated within a Simulink subsystem block, as illustrated in Fig. 3.

Table I. Parameters of the plant model for human lower limb motion

Segment	Parameter	Symbol	Value	Unit
Thigh	Mass	m_1	$0,1 \cdot M$	[kg]
	Length	L_1	$0,284 \cdot H$	[m]
	Proximal center of gravity	l_1	$0,433 \cdot L_1$	[m]
	Radius of gyration	k_1	$0,540 \cdot L_1$	[m]
	Moment of inertia	J_1	$m_1 \cdot k_1^2$	[kg · m ²]
	Viscous damping coefficient	b_1	0.1	[N · m · s]
Lower leg	Mass	m_2	$0,0465 \cdot M$	[kg]
	Length	L_2	$0,246 \cdot H$	[m]
	Proximal center of gravity	l_2	$0,433 \cdot L_2$	[m]
	Radius of gyration	k_2	$0,528 \cdot L_2$	[m]
	Moment of inertia	J_2	$m_2 \cdot k_2^2$	[kg · m ²]
	Viscous damping coefficient	b_2	0.1	[N · m · s]
Foot	Mass	m_3	$0,0145 \cdot M$	[kg]
	Length	L_3	$0,152 \cdot H$	[m]
	Proximal center of gravity	l_3	$0,5 \cdot L_3$	[m]
	Radius of gyration	k_3	$0,690 \cdot L_3$	[m]
	Moment of inertia	J_3	$m_3 \cdot k_3^2$	[kg · m ²]
	Viscous damping coefficient	b_3	0.1	[N · m · s]

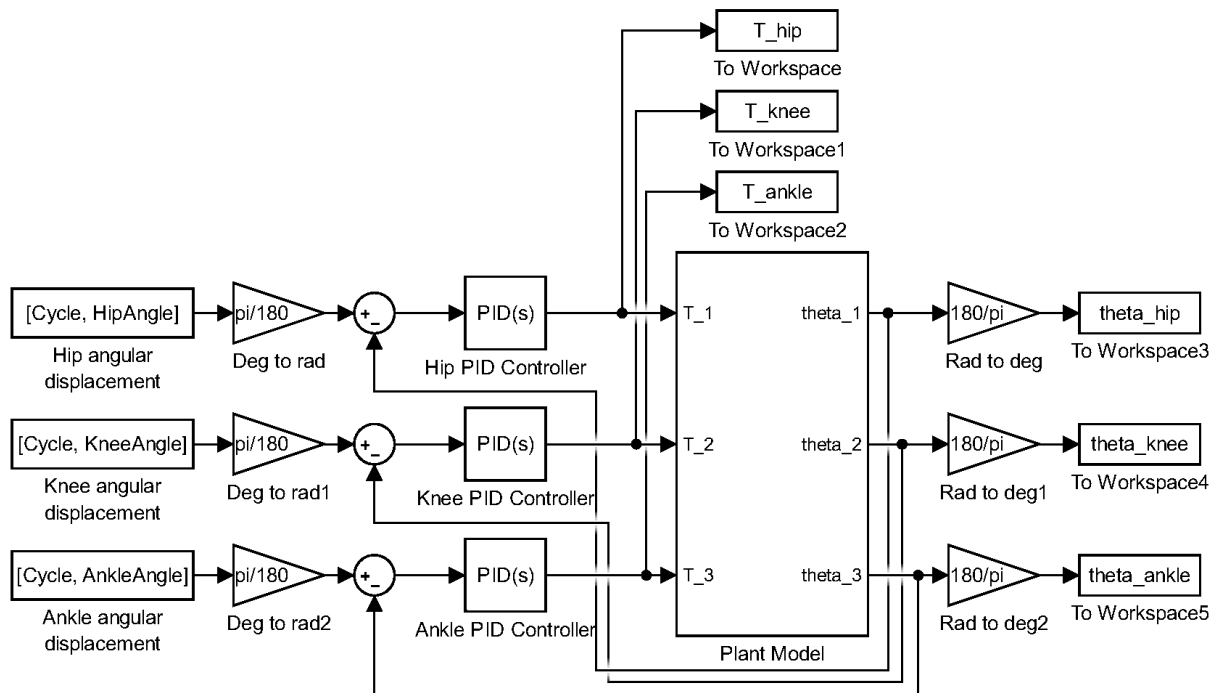


Figure 3. Closed-loop PID controllers implemented in the plant model in Simulink

A notable aspect of this modeling process pertains to unit conversions. While the plant model operates with angular displacements measured in radians, reference trajectories are presented in degrees. To ensure consistency, unit conversion is performed using specialized gain blocks designated as *Deg to rad* and *Rad to deg*. These blocks facilitate the transformation of reference trajectories from degrees to radians before tracking error computation. Furthermore, the angular displacements of the dynamic model are converted from radians to degrees for visualization purposes.

PID control is a classical closed-loop control technique defined by the Laplace domain transfer function shown in Eq. (29). It comprises three essential constants: proportional K_p , integral K_i , and derivative K_d . These constants play distinct roles in shaping system behavior: the proportional constant enhances the system's responsiveness; the integral constant reduces steady-state error; improving precise tracking of reference trajectories; and the derivative constant manages the tracking error's evolution over time (2).

$$PID(s) = K_p + \frac{K_i}{s} K_d s \quad (29)$$

To optimize controller performance, an experimental tuning process was conducted on the plant model. The objective was to achieve optimal tracking performance while ensuring that joint torques remained within the reported maximum values for normal gait (29). The tuning process resulted in PD controllers for the three joints, configured as follows: the hip controller was configured with $K_p = 10,000$ and $K_d = 1$, the knee controller with $K_p = 1,000$ and $K_d = 10$, and the ankle controller with $K_p = 1,000$ and $K_d = 10$.

3. Simulations and results

Simulations of the dynamic model were conducted using human gait reference trajectories obtained from (29), with due consideration to the anthropometric data (body mass and height) reported in their research. These reference trajectories comprise the angular displacement of the hip, knee, and ankle joints during the gait cycle of healthy male adults.

Graphical simulation results are presented in Figs. 4, 5, and 6, each consisting of three plots corresponding to the three lower limb joints: (a) hip, (b) knee, and (c) ankle. Fig. 4 shows the tracking of angular displacement, with the reference trajectory represented as the dotted line and the angular displacement of the segment in the dynamic model shown as the solid line. Fig. 5 illustrates the tracking error regarding angular displacement, calculated as the difference between the reference trajectory and the angular displacement of the segment. Fig. 6 presents the normalized joint torque during the execution of the desired gait reference trajectory. This normalization is established relative to the individual's body mass.

The assessment of angular displacement tracking in the dynamic model involved the application of two key metrics: the relative maximum error (RME) and the root mean square error (RMSE), both in magnitude and as a percentage. These metrics were calculated using Eqs. (30) to (33), where θ_d represents the reference trajectory, θ_n signifies the angular displacement of the segment in the dynamic

model, and N denotes the signal length (2). Quantitative results from this evaluation are presented in Table II, encompassing data for the three segments under consideration.

Table II. Angular displacement tracking errors of the dynamic model

Segment	RME [°]	% RME	RMSE [°]	% RMSE
Thigh	0,649	1,924	0,240	1,100
Lower leg	2,161	3,410	0,795	2,567
Foot	0,310	0,322	0,125	0,139

$$RME = \max|\theta_d - \theta_n| \quad (30)$$

$$\%RME = \frac{\max|\theta_d - \theta_n|}{\max|\theta_d|} \cdot 100 \quad (31)$$

$$RMSE = \sqrt{\frac{1}{N} \sum (\theta_d - \theta_n)^2} \quad (32)$$

$$\%RMSE = \frac{\sqrt{\frac{1}{N} \sum (\theta_d - \theta_n)^2}}{\sqrt{\frac{1}{N} \sum (\theta_d)^2}} \cdot 100 \quad (33)$$

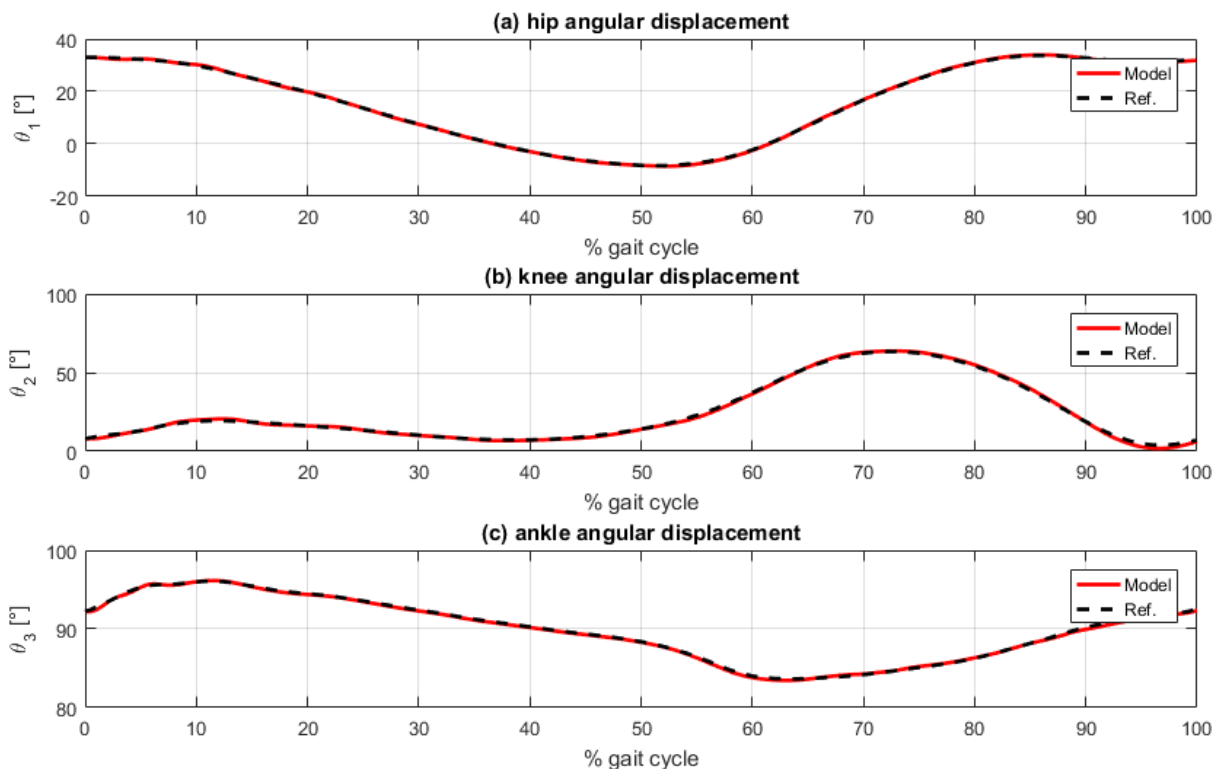


Figure 4. Angular displacement tracking: (a) hip, (b) knee, and (c) ankle

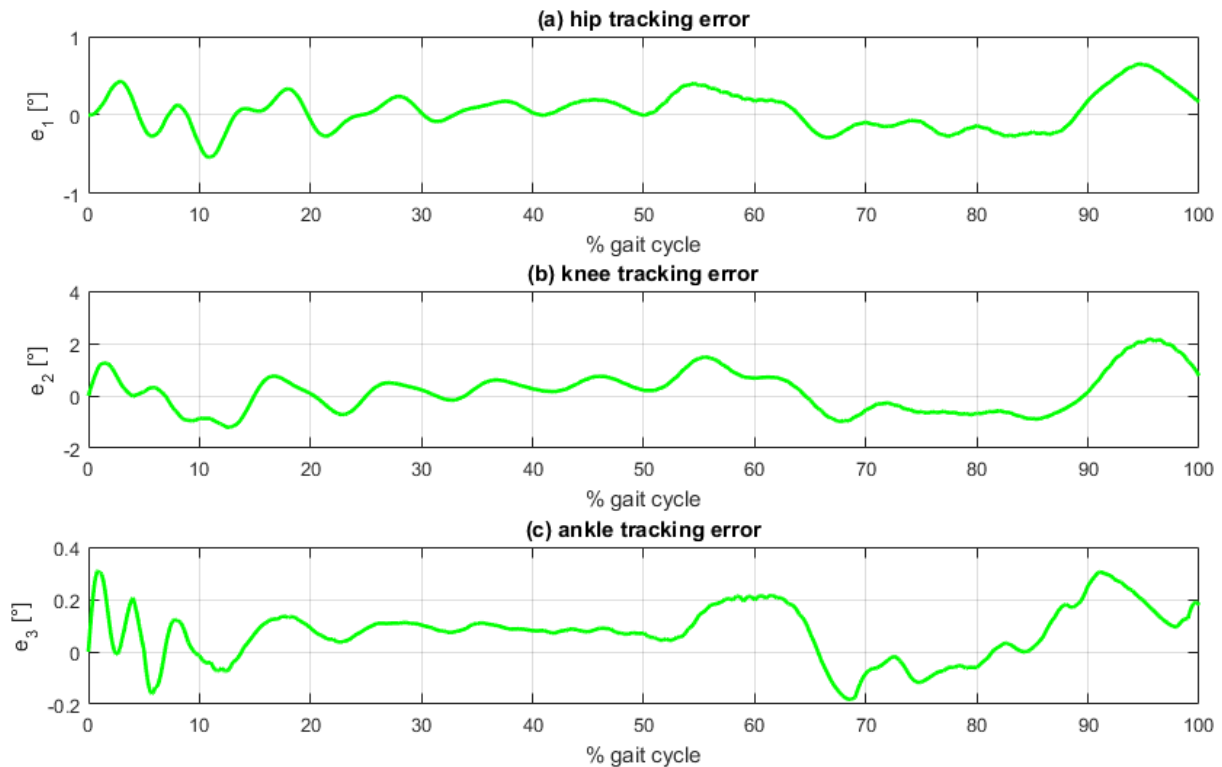


Figure 5. Angular displacement tracking error: (a) hip, (b) knee, and (c) ankle

The analysis of the graphical results, as depicted in Figs. 4 and 5, reveals that the most significant tracking errors tend to appear during the peaks of the reference trajectories. While PID controllers can be finetuned to minimize tracking errors, it is essential to recognize that pushing these controllers to achieve such minimal errors could result in joint torques surpassing the reported values for normal human gait (29).

Angular displacement tracking was effectively accomplished with errors remaining under 2.2 [°] in magnitude and within a margin of 3,5% for all three segments considered. Notably, the lower leg segment exhibited the most substantial tracking errors. This can be attributed to the dynamic interactions between the thigh and foot segments, which, in turn, impact the lower leg's overall performance. Despite these challenges, the tracking errors for the thigh and foot segments were effectively constrained below 0,65 [°] and 2%.

4. Conclusions

This paper presented the development of a dynamic model for human lower limb motion in the sagittal plane during the gait cycle. The dynamic model was composed of two primary components: (1) the plant model and (2) a closed-loop PID controller. The plant model served as the foundation for understanding the forward dynamics of human gait. It was constructed based on a multi-mass pendulum, encompassing three lower limb segments (thigh, lower leg, and foot) and three joints (hip,

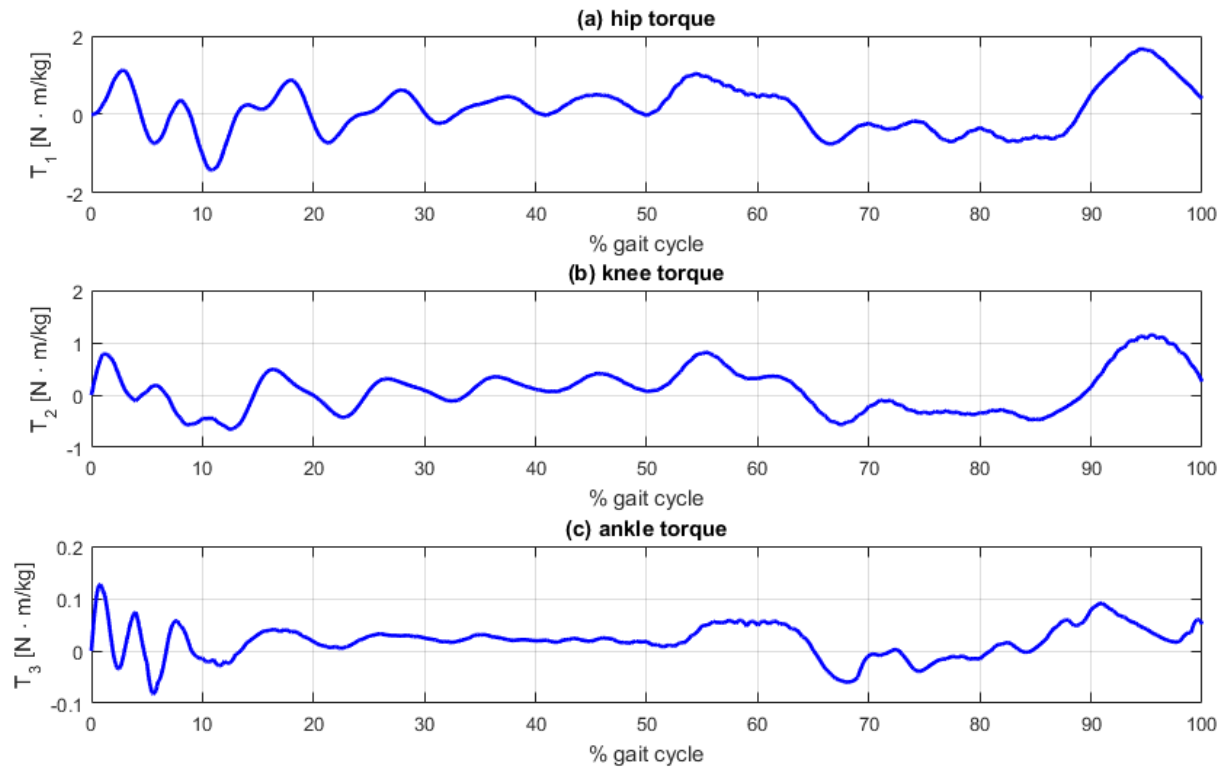


Figure 6. Joint torque: (a) hip, (b) knee, and (c) ankle

knee, and ankle). The governing nonlinear second-order differential equations of the plant model were derived through Euler-Lagrange formulation and subsequently implemented in MATLAB's Simulink. To replicate human gait reference trajectories and simulate the functioning of the neuromusculoskeletal system and the CNS, a closed-loop PID controller was integrated to the plant model for tracking angular displacement.

Simulations were conducted using human gait reference trajectories sourced from healthy adult males. The accuracy of angular displacement tracking was rigorously assessed, quantified by two key metrics: the relative maximum error (RME) and the root mean square error (RMSE). The simulation results affirm the reliability of the dynamic model, demonstrating its ability to faithfully reproduce human gait trajectories with a high degree of precision. The errors observed were consistently below $2,2 [^\circ]$ in magnitude and $3,5\%$ for all three considered segments (thigh, lower leg, and foot).

Within the domain of dynamic human gait modeling, this model resides within the realm of biped robotics, offering a unique hybrid approach that amalgamates pendulum and control-based methodologies. This model stands as a potent tool, empowering the design of rehabilitation and assistive devices, such as exoskeletons, prostheses, and orthoses. It enables crucial functionalities, including joint torque estimation, analysis of kinematic variables, optimal actuator selection, and exploration of advanced control techniques.

5. Author contributions

José Luis Sarmiento-Ramos: Conceptualization, investigation, software, supervision, writing – original draft, writing – review and editing.

Andrés Felipe Meneses-Castro: Investigation, software, writing – original draft.

Pedro José Jaimes-Mantilla: Investigation, software, writing – original draft.

References

- [1] C. A. Oatis, *Kinesiology: the mechanics and pathomechanics of human movement*, 2nd ed., USA: Lippincott Williams and Wilkins, 2009. ↑3, 5
- [2] J. L. Sarmiento-Ramos, A. P. Rojas-Ariza and Y. Z. Rueda-Parra, “Dynamic model of flexion/extension and abduction/adduction of the shoulder joint complex,” in *2021 IEEE 2nd Int. Cong. Biomed. Eng. Bioeng.*, 2021, pp. 1-4. <https://doi.org/10.1109/CI-IBBI54220.2021.9626105> ↑3, 12, 13
- [3] J. L. Sarmiento-Ramos and M. F. Anaya-Rojas, “Modelling, design and construction of a wrist rehabilitation exoskeleton,” *Scientia et Technica*, vol. 27, no. 3, pp. 177-185, Sept. 2022. <https://doi.org/10.22517/23447214.24748> ↑3
- [4] J. L. Sarmiento-Ramos, J. C. Suárez-Galvis and V. Grisales-Muñoz, “Exoskeleton for ankle joint flexion/extension rehabilitation,” *ITECKNE*, vol. 19, no. 2, art. 2773, Jun. 2022. <https://doi.org/10.15332/iteckne.v19i2.2773> ↑3
- [5] J. Sun, “Dynamic modeling of human gait using a model predictive control approach,” Ph.D. dissertation, Fac. of the Grad. Sch., Marquette Univ., Milwaukee, USA, 2015. [Online]. Available: https://epublications.marquette.edu/cgi/viewcontent.cgi?referer=&httpsredir=1&article=1481&context=dissertations_mu ↑3, 4
- [6] F. De Groote and A. Falisse, “Perspective on musculoskeletal modelling and predictive simulations of human movement to assess the neuromechanics of gait,” *Proc. R. Soc. B.*, vol. 288, art. 2432, Mar. 2021. <https://doi.org/10.1098/rpsb.2020.2432> ↑3
- [7] Y. Xiang, J. S. Arora and K. Abdel-Malek, “Physics-based modeling and simulation of human walking: A review of optimization-based and other approaches,” *Struc. Multidisc. Optim.*, vol. 42, pp. 1-23. 2010. <https://doi.org/10.1007/s00158-010-0496-8> ↑3, 4
- [8] F. L. Buczek, K. M. Cooney, M. R. Walker, M. J. Rainbow, M. C. Concha and J. O. Sanders, “Performance of an inverted pendulum model directly applied to normal human gait,” *Clin. Biomech.*, vol. 21, no. 3, pp. 288-296, 2006. <https://doi.org/10.1016/j.clinbiomech.2005.10.007> ↑3
- [9] P. Sun, Y. Gu, H. Mao, Z. Chen and Y. Li, “Research on walking gait planning and simulation of a novel hybrid biped robot,” *Biomimetics*, vol. 8, no. 2, art. 258, 2023. <https://doi.org/10.3390/biomimetics8020258> ↑3

- [10] G. Yu, J. Zhang and W. Bo, "Biped robot gait planning based on 3D linear inverted pendulum model," *IOP Conf. Ser.: Mater. Sci. Eng.*, vol. 301, art. 012098, 2018. <https://doi.org/10.1088/1757-899X/301/1/012098> ↑3
- [11] T. Dong, D. Wang and D. Zhao, "Gait research and simulation analysis of biped robot," in *Proc. SPIE 12305 Int. Symp. Artif. Intell. App. Tech.*, art. 123050A, 2022. <https://doi.org/10.1117/12.2645550> ↑3
- [12] Y. Liu, S. Peng, Y. Du, and W. H. Liao, "Kinematics modeling and gait trajectory tracking for lower limb exoskeleton robot based on PD control with gravity compensation," in *Proc. 38th Chin. Ctrl. Conf.*, 2019, pp. 4504-4511. <https://doi.org/10.23919/ChiCC.2019.8865916> ↑3
- [13] G. Marconi, A. A. Gopalai and S. Chauhan, "A triple compound pendulum model to analyze the effect of an ankle-foot orthosis on swing phase kinematics," *Med. Eng. Phys.*, vol. 112, art. 103951, 2023. <https://doi.org/10.1016/j.medengphy.2023.103951> ↑3
- [14] M. Irine. R. Hirouji, D. Ura, K. Osuka and T. Kinugasa, "Experimental verification of the characteristic behaviors in passive dynamic walking," *Art. Life Robot.*, vol. 26, pp. 187 – 194, 2021. <https://doi.org/10.1007/s10015-020-00670-y> ↑3
- [15] S. Montazeri, M. Sadeghi, A. Niaty, F. Towhidkhan and S. Jafari, "The simple chaotic model of passive dynamic walking," *Nonlinear Dyn.*, vol. 93, no. 3, pp-1183-1199, 2018. <https://doi.org/10.11007/s11071-018-4252-8> ↑3
- [16] E. Added, H. Gritli and S. Belghith, "Further analysis of the passive dynamics of the compass biped walker and control of chaos via two trajectory tracking approaches," *Complexity*, vol. 2021, art. 5533451, 2021. <https://doi.org/10.1155/2021/5533451> ↑3
- [17] C. Dinesh, M. Deivakani, P. Sunagar, R. Baskar, A. Kumar and G. Kalra, "Biped robot-based walking on uneven terrain: Stability and zero moment point (ZMP) analysis," *AIP Conf. Proc.*, vol. 2831, no. 1, art. 020013, 2023. <https://doi.org/10.1063/5.0162762> ↑4
- [18] A. Fawzi Abdul Kareem and A. Abdul Hussein Ali, "Experimental and theoretical optimal regulator control of balance zero moment point for bipedal robot," *J. Eng. Sustain. Dev.*, vol. 24, no. 6, pp. 68- 82, 2020. <https://doi.org/10.31272/jeasd.24.6.6> ↑4
- [19] Y. D. Hong, "Capture point-based controller using real-time zero moment point manipulation for stable bipedal walking in human environment," *Sensors*, vol. 19, no. 15, art. 3407, 2019. <https://doi.org/10.3390/s19153407> ↑4
- [20] B. Ren, J. Liu and J. Chen, "Simulating human-machine coupled model for gait trajectory optimization of the lower limb exoskeleton system based on genetic algorithm," *Int. J. of Adv. Robot. Sys.*, vol. 17, no. 1, 2020. <https://doi.org/10.1177/1729881419893493> ↑4
- [21] M. A. Khan, H. Arshad, R. Damasevicius A. Alqahtani, S. Alsubai, A. Binbusayyis, Y. Nam and B. Kang, "Human gait analysis: a sequential framework of lightweight deep learning and improved moth-flam optimization algorithm," *Comput. Intell. Neurosci.*, vol. 2022, art. 8238375, 2022. <https://doi.org/10.1155/2022/8238375> ↑4
- [22] J. Sun, S. Wu and P. A. Voglewede, "Dynamic simulation of human gait model with predictive capability," *ASME J. Biomech. Eng.*, vol. 140, no. 3, art. 031008, 2018. <https://doi.org/10.1115/1.4038739> ↑4

- [23] J. G. Juang, "Fuzzy neural network approaches for robotic gait synthesis," *IEEE Trans. Syst. Man. Cybern.*, vol. 30, no. 4, pp. 594-601, 2004. <https://doi.org/10.1109/3477-.865178> ↑4
- [24] M. L. Felis, K. Mombaur and A. Berthoz, "An optimal control approach to reconstruct human gait dynamics from kinematic data," in *2015 IEEE-RAS 15th Int. Conf. Humanoid Rob.*, pp. 1044-1051, 2015. <https://doi.org/10.1109/HUMANOIDS.2015.736490> ↑4
- [25] T. Saidouni and G. Bessonnet, "Generating globally optimized sagittal gait cycles of a biped robot," *Robotica*, vol. 41, no. 3, pp. 465-479, Jul. 2010. <https://doi.org/10.1007/s00158-009-0423-z> ↑4
- [26] D. A. Winter, *Biomechanics and motor control of human movements*, USA: John Wiley and Sons, Inc., 2009. ↑9
- [27] Y. Li, C. Xu and X. Guan, "Modeling and simulation study of electromechanically system of the human extremity exoskeleton," *J. Vibroengineering*, vol. 18, no. 1, pp. 551-561, Feb. 2016. [Online]. Available: <https://www.extrica.com/article/16394> ↑9
- [28] M. Oluwatsin, "Modelling and control of actuated lower limb exoskeletons: a mathematical application using central patterns generators and nonlinear feedback control techniques," Ph.D. dissertation, Univ. Paris-Est Et Mstic, 2016. Available: <https://tel.archives-ouvertes.fr/tel-01531927/document> ↑9
- [29] G. Bovi, M. Rabuffetti, P. Mazzoleni and M. Ferrarin, "A multiple-task gait analysis approach: kinematic, kinetic and EMG reference data for healthy young and adult subjects," *Gait Post.*, vol. 33, no. 1, pp. 6-13, Jan. 2011. <https://10.1016/j.gaitpost.2010.08.009> ↑12, 14

José Luis Sarmiento-Ramos

Mechanical Engineer and Master of Science in Mechanical Engineering from Universidad Industrial de Santander, Bucaramanga, Colombia. From 2015 to 2016, he served as a Teaching Assistant in the School of Mechanical Engineering at Universidad Industrial de Santander, Bucaramanga, Colombia. From 2019 to 2022, he worked as Professor and Researcher in the Department of Biomedical Engineering at Universidad Manuela Beltrán, Bucaramanga, Colombia. From 2022 to 2023, he worked as Professor in the Faculty of Mechatronic Engineering at Universidad Santo Tomás, Bucaramanga, Colombia. He has also worked as a Guest Lecturer for the Master's degree in Hydraulics at Universidad Técnica de Manabí, Portoviejo, Ecuador. Currently, he works as CNC Manufacturing Manager at Rambal S.A.S BIC, Bucaramanga, Colombia. His current research interests include biomechanics, dynamic systems, fluid power servo systems, and control engineering.

Email: jefe.fabricacioncnc@rambal.com.co

Andrés Felipe Meneses-Castro

Biomedical Engineering student from Universidad Manuela Beltrán, Bucaramanga, Colombia. His current research interests include biomechanics, dynamic systems, and control engineering.

Email: andres.meneses@academia.umb.edu.co

Pedro José Jaimes-Mantilla

Biomedical Engineering student from Universidad Manuela Beltrán, Bucaramanga, Colombia. His current research interests include biomechanics, dynamic systems, and control engineering.

Email: pedro.jaimes@academia.umb.edu.co

